Leaf-level metabolic changes in response to drought affect daytime CO_2 emission and isoprenoid synthesis pathways

S. Nemiah Ladd[1, 2, *, #], L. Erik Daber[1, *], Ines Bamberger[1, a], Angelika Kübert[1, b], Jürgen Kreuzwieser[1], Gemma Purser[3, 4], Johannes Ingrisch[1, 5], Jason Deleeuw[6], Joost van Haren[6, 7], Laura K. Meredith[6, 8], Christiane Werner[1]

[1] Ecosystem Physiology, University of Freiburg, Georges-Köhler-Allee 053/054, 79110 Freiburg, Germany

[2] Department of Environmental Sciences, University of Basel, Bernoullistrasse 30, 4056 Basel, Switzerland

[3] School of Chemistry, The University of Edinburgh, Joseph Black Building, David Brewster Road, Edinburgh, EH9 3FJ, UK

[4] UK Centre for Ecology & Hydrology, Bush Estate, Penicuik, EH26 0QB, U K

[5] Department of Ecology, University of Innsbruck, Sternwartestrasse 15, 6020 Innsbruck, Austria

[6] Biosphere 2, University of Arizona, 32540 S. Biosphere Rd., Oracle, AZ, 85739, USA

[7] Honors College, University of Arizona, 1101 E. Mabel Street, Tucson, AZ, 85719, USA

[8] School of Natural Resources and the Environment, University of Arizona, Tucson, AZ, USA

*Equal contributions

[#]Corresponding author. Address for correspondence: Department of Environmental Sciences, University of Basel, Bernoullistrasse 30, 4056 Basel, Switzerland. Email: n.ladd@unibas.ch; phone: + 41 61 207 3636

[a] Current address: Atmospheric Chemistry Group, University of Bayreuth (BayCEER), Dr-Hans-Frisch-Straße 1-3, 95448 Bayreuth, Germany

[b] Current address: Institute for Atmospheric and Earth System Research, University of Helsinki, Pietari Kalmin katu 5, 00014 Helsinki, Finland

Keywords daytime respiration, drought, GC-IRMS, isoprenoids, legumes, position-specific isotope labeling, PTR-ToF-MS, tropical plants, volatile organic compounds

Abstract

In the near future, climate change will cause enhanced frequency and/or severity in terrestrial ecosystems, including tropical forests. Drought responses by tropical trees may affect their carbon use, including production of volatile organic compounds (VOCs), with unpredictable implications for carbon cycling and atmospheric chemistry. It remains unclear how metabolic adjustments by mature tropical trees in response to drought will affect their carbon fluxes associated with daytime CO_2 production and VOC emission. To address this gap, we used position-specific ^{13}C-pyruvate labeling to investigate leaf CO_2 and VOC fluxes from four tropical species before and during a controlled drought in the enclosed rainforest of Biosphere 2. Overall, plants that were more sensitive to drought had greater reductions in daytime CO_2 production. Although daytime CO_2 production was always dominated by non-mitochondrial processes, the relative contribution of CO_2 from the tricarboxylic acid cycle tended to increase under drought. A notable exception was the legume tree *Clitoria fairchildiana,* which had less anabolic CO_2 production than the other species even under pre-drought conditions, perhaps due to more efficient refixation of CO_2 and anaplerotic use for amino acid synthesis. *C. fairchildiana* was also the only species to allocate detectable amounts of ^{13}C label to VOCs, and was a major source of VOCs in the Biosphere 2 forest. In *C. fairchildiana* leaves, our data indicate that intermediates from the mevalonic acid pathway are used to produce the volatile monoterpene trans-β-ocimene, but not isoprene. This apparent crosstalk between the mevalonic acid and methylerythritol phosphate pathways for monoterpene synthesis declined with drought. Finally, although trans-β-ocimene emissions increased under drought, it was increasingly sourced from stored intermediates and not *de novo* synthesis. Unique metabolic responses of legumes may play a disproportionate role in the overall changes in daytime CO_2 and VOC fluxes in tropical forests experiencing drought.

Introduction

Due to anthropogenic climate change, the frequency and/or intensity of droughts are expected to increase, particularly in tropical regions (Douville et al., 2021). The responses of tropical forests to droughts can have important feedbacks on the global carbon cycle, as these forests represent a significant carbon sink today, but may lose that capacity as warming and droughts increase (Mitchard 2018; Hubau et al., 2020). Additionally, tropical forests are an important source of volatile organic compounds (VOCs) to the atmosphere (Guenther et al., 2006). The overall fluxes and molecular composition of VOCs emitted from tropical forests are also likely to change with increased drought (Peñuelas and Llusia, 2003), with further implications for atmospheric chemistry (Atkinson and Arey, 2003; Claeys et al., 2004; Lelieveld et al., 2008). It is therefore important to better characterize and understand changes in carbon fluxes, including allocation to VOCs, on an ecosystem and individual tree scale in tropical forests in response to drought.

In depth investigations of drought in natural forests remain challenging, since the timing of severe droughts is difficult to predict in advance and it is rarely practical to leave extensive analytical equipment in place for long periods of time in the hopes of capturing an extreme event. Model ecosystems such as the enclosed tropical rainforest in the Biosphere 2 (B2) experimental facility in Oracle, AZ, USA, thus provide a valuable means to experimentally investigate drought impacts in a near-natural setting (Rascher et al., 2004; Pegoraro et al., 2006; Evaristo et al., 2019; Werner et al., 2021). In 2019, the Biosphere 2 Water Atmosphere and Life Dynamics (B2WALD) campaign made use of this unique experimental ecosystem to investigate drought from molecular to ecosystem scales by subjecting it to a two-month drought accompanied by intensive *in situ* measurements and sampling of different ecosystem components before, during, and after drought (Werner et al., 2021). Among other findings, initial analyses from the B2WALD campaign demonstrated

that overall ecosystem fluxes of water, CO_2, and VOCs were influenced in different ways by four distinct functional plant groups: drought-sensitive and drought-tolerant canopy trees, and drought-sensitive and drought-tolerant understory plants (Werner et al., 2021, for further details, see **Figure 1**). While it is clear that overall changes in ecosystem CO_2, water, and VOC fluxes were driven by differing responses from these four plant functional groups during the B2WALD drought, the specific metabolic adjustments within each of these four plant groups have not yet been investigated. In particular, changes in leaf gas exchange, water use efficiency, and partitioning of carbon between catabolic and anabolic processes, including the biosynthesis of VOCs, could potentially provide valuable insight into how and why plant functional groups adjusted their metabolism towards drought.

To investigate metabolic adjustments towards drought and how they relate to the diverse drought responses of different plant functional groups, we measured the incorporation of ^{13}C from position-specific pyruvate labels into CO_2 and VOCs before and during the B2WALD drought. This approach is based on the fact that different carbon atoms within the central metabolite pyruvate are used for distinct biochemical processes. For example, carbon atoms from the C2 and C3 positions of pyruvate are converted to CO_2 by respiration in the tricarboxylic acid (TCA) cycle (**Figure 2, step 1**) (Tcherkez et al., 2005; Priault et al., 2009), while carbon atoms from the C1 position of pyruvate are also released due to TCA cycle activity (**Figure 2**) (Tcherkez et al., 2008; Priault et al., 2009). However, numerous non-mitochondrial anabolic processes also decarboxylate the C1 position of pyruvate, while the C2 and C3 position are incorporated into biosynthetic products (**Figure 2**) (Graus et al., 2004; Schnitzler et al., 2004; Jardine et al., 2010). Together, these processes cause greater ^{13}C enrichment of CO_2 following labeling with $^{13}C1$-pyruvate than ^{13}C enrichment of CO_2 following labeling with $^{13}C2$-pyruvate during the day, when the TCA cycle is downregulated (Tcherkez et al., 2008; Priault et al., 2009). The relative difference in ^{13}C enrichment of CO_2

following labeling with each type of pyruvate is thus broadly indicative of the relative significance of CO_2 production from non-mitochondrial anabolic processes (Priault et al., 2009; Werner et al., 2009; Tcherkez et al., 2012; Fasbender et al., 2018).

Position-specific ^{13}C labeling can also be employed to study the synthesis of various plant metabolites, including VOCs (Schwender et al., 1996; Lichtenthaler et al., 1997; Schuhr et al., 2003; Fasbender et al., 2018; Werner et al., 2020). This approach can be particularly helpful for understanding the biosynthesis of both volatile and non-volatile isoprenoids, and for assessing the role of metabolic crosstalk between the cytosolic mevalonic acid (MVA) and the plastidic methylerythritol phosphate (MEP) pathways for isoprenoid biosynthesis (**Figure 2, step 4 & 5**) (Schuhr et al., 2003; Massé et al., 2004; Werner et al., 2020; Ladd et al., 2021).

While position-specific ^{13}C labeling is well established in laboratory experiments on potted plants, no study has used this approach to assess metabolic adjustments of mature plants in response to drought in a natural ecosystem. Based on the initial characterization of four functional groups in the B2 rainforest, we labeled leaves from *Clitoria fairchildiana* R.A. Howard (drought-sensitive canopy), *Phytolacca dioica* L. (drought-tolerant canopy), *Hibiscus rosa sinensis* L. (drought-tolerant understory), and *Piper auritum* Kunth (drought-sensitive understory) with position-specific ^{13}C-pyruvate before and during the B2WALD drought to address the following hypotheses: (1) drought-sensitive plants with large reductions in assimilation and transpiration also produce and release less CO_2 from pyruvate, as their overall metabolism slows, (2) the majority of cytosolic pyruvate is used for non-mitochondrial processes in the light under control conditions, but the difference with use in the TCA cycle declines as drought responses intensify, and (3) for isoprenoid emitting plants, the proportion of isoprenoids synthesized from cytosolic pyruvate increases under drought in drought-sensitive plants as the supply of fresh photosynthate available for biosynthesis

declines. Together, this approach allows us to evaluate how allocation of pyruvate changed under drought, and how these metabolic adjustments relate to the diverse integrated drought responses of each of these four tropical plant species.

Materials and Methods

Drought campaign

This study took place within the context of the broader B2WALD campaign, described in detail by Werner et al. (2021). The B2WALD campaign made use of the enclosed rainforest that has been growing continuously for over 30 years at the B2 research facility, located north of Tucson, AZ, USA. The enclosed system is equipped with sprinklers that control precipitation within the forest, thus enabling full control over the start and end dates for the drought experiment. Additionally, temperature and ambient CO_2 concentrations within the forest are elevated compared to natural tropical rain forests, making this system a potential analogue for future climate scenarios (Lloyd and Farquhar, 2008). In 2019, this mature ecosystem was subjected to a 65-day drought, with intensive monitoring of gas fluxes from leaves, stems, soils, and roots throughout a 110-day period before, during, and after drought (Werner et al., 2021). Under non-drought conditions, the Biosphere 2 rainforest receives 1600 mm/year, distributed by overhead sprinklers three times per week. Following the final pre-drought rain event on the night of 7 October 2019, we turned off the sprinkler system and did not add additional water to the system until 2 December 2019. Daytime temperature within the canopy of the Biosphere 2 rainforest ranged from 23.3 to 33.5 °C during the pre-drought period and 22.2 to 34.8 °C during the drought. Corresponding daytime temperature ranges for the understory were 21.3 - 26.6 °C and 22.2 - 29.6 °C, respectively. maximum photosynthetically active radiation (PAR) values outside the enclosure declined from 1685 to 1016 μmol m^{-2} s^{-1} (Werner et al., 2021).

During the first four weeks of the B2WALD drought, surface soil moisture was almost completely depleted, and the atmospheric vapor pressure deficit increased in both the canopy and the understory, but at a higher rate in the canopy (Werner et al., 2021). In normal years there is no seasonal variability in precipitation within the Biosphere 2 rainforest, and the ecosystem-scale changes in water and carbon fluxes were much stronger than seasonal changes associated with reduced external light availability. Changes in water fluxes by individual plants were also clearly driven primarily by drought and not light availability, as the trees' sap flow increased immediately when rain first returned to the system in mid-December, when ambient light levels were at their annual minimum.

Gas sampling system and analyzers

For all target species (*Clitoria fairchildiana*, *Piper auritum*, *Phytolocca dioica* and *Hibiscus rosa sinensis*), we enclosed whole leaves in species-specific, flow-through ventilated cuvettes made from FEP film and PFA tubing as described in Kübert et al. (2023). One end of the leaf cuvette was sealed around the petiole, while the other end was sealed around the incoming and outcoming PFA tubes. For *H. rosa sinensis*, we used cuvettes that enclosed several leaves on terminal branches. This was necessary because it was difficult to avoid embolism when cutting the petiole of single *H. rosa sinensis* leaves. We equipped each cuvette with a data logger and a light sensor that recorded light levels at an angle parallel to the leaf's surface, as well as a thermocouple that recorded leaf surface temperature. Leaf temperature inside the leaf cuvettes did not exceed daytime ecosystem temperature maxima reported in Werner et al. (2021) (**Table S1**).

We continuously supplied each cuvette with a mix of VOC- and CO_2-free air produced by a zero air generator (Aadco Instruments, Inc., Cleves, OH, USA) and a constant amount of CO_2 (~500 ppm, $\delta^{13}C$ ~ -10 ‰) from a gas tank. This relatively high CO_2

concentration was selected to match the average ambient concentrations within the Biosphere 2 rainforest. Each cuvette was equipped with a fan to guarantee efficient air mixing. The outflow from the cuvette was connected to a Teflon T-piece and ball valve that allowed us to sample a portion of the flow onto cartridges for offline VOC analyses (details below). Additional flow was diverted to three analyzers: (1) a proton transfer reaction – time of flight mass spectrometer (PTR-TOF-MS 4000ultra, Ionicon Analytic, Innsbruck, Austria) for VOC fluxes, (2) a carbon isotope laser spectrometer (Delta Ray IRIS, Thermo Fisher Scientific, Bremen, Germany) for concentrations and stable isotopes of CO_2, and (3) a water isotope cavity ring-down spectrometer (L2120i water isotope analyzer, Picarro Inc., Santa Clara, CA, USA) for concentrations and stable isotopes of water vapor. Details of the gas sampling system, analyzers, and the calibration of different analyzers used during the B2WALD campaign are provided in Werner et al. (2021).

Position-specific ^{13}C-pyruvate labeling

We conducted position-specific ^{13}C-pyruvate labeling during two time periods: pre-drought (12 – 28 September 2019) and drought (4 – 16 November, 2019; after 27 – 39 days without rain), using a protocol similar to that of Fasbender et al. (2018). For canopy trees, we did the labeling during the morning hours, when overall photosynthesis tends to be highest in the B2 rainforest, as hot temperature in the sunlit canopy induce early stomatal closures (Rascher et al., 2004; Rosolem et al., 2010). For the cooler understory, we primarily labeled in the afternoon. Leaves were installed in cuvettes at least one day prior to the labeling event. Immediately prior to labeling, we monitored the cuvette for 15 minutes to ensure that leaf fluxes of CO_2 and VOCs were stable. We then cut the leaf petiole and rapidly placed it under water, and cut it again to avoid embolism. The petiole remained in a 1.5 mL centrifuge tube filled with water for five more minutes so that the fluxes could stabilize after cutting.

209 Subsequently, we exchanged the centrifuge tube with one containing a 10 mM solution of
210 either ^{13}C1- or ^{13}C2-pyruvate (99 atom % ^{13}C, Cambridge Isotope Laboratories, Andover,
211 MA, USA). We used the mass decline of the centrifuge tube over time to calculate the label
212 uptake. In most cases, leaf fluxes of H_2O, CO_2, and VOCs returned to the levels they had
213 while attached to the plant soon after cutting. The few leaves that did not stabilize at or near
214 their previous gas fluxes after being placed in the label solution were excluded from
215 subsequent analyses.

216 We collected the leaf after each measurement to determine its leaf area by tracing it
217 on a sheet of paper of known surface density and weighing the leaf's shape on a fine mass-
218 balance. We filled missing leaf area values with the median value of all leaves of the same
219 species (n = 16).

220

221 *Cartridge sampling and analyses*

222 To further identify and quantify the specific monoterpenes emitted from leaves, we
223 collected monoterpenes on glass cartridges filled with Tenax during each pyruvate labeling
224 event. We used an air sampling pump (220-1000TC, SKC, Eighty Four, PA, USA) attached
225 at the outlet to maintain a defined air flow (100 - 200 ml min^{-1}) through the cartridge. We
226 attached the cartridges to the cuvette for at least 30 minutes prior to the leaf cutting and for
227 ~70 minutes while the leaf petiole was submersed in the pyruvate solution. Parallel to the
228 collection of each cartridge from the leaf cuvette, we collected a cartridge from the empty
229 cuvette to correct for cuvette background and potential contaminants. After sample collection
230 we sealed the cartridges in vacutainers and stored them at room temperature prior to analysis.

231 We subsequently analyzed all cartridge samples by gas chromatography – mass
232 spectrometry – combustion interface – isotope ratio mass spectrometry (GC-MS – C – IRMS)
233 at the University of Freiburg to identify and quantify the emitted VOCs and to determine the

$\delta^{13}C$ values of individual VOCs. Volatiles were analyzed after thermodesorption on a GC (7890B, Agilent Technologies Böblingen, Germany) equipped with a mass-selective detector (MSD, 5975C, Agilent Technologies Böblingen, Germany) and a thermodesorption/cold injection system (TDU-CIS4, Gerstel, Germany). VOCs were desorbed from cartridges at 220 °C and immediately trapped in the CIS at −70°C. The CIS was heated to 240 °C, channeling the volatiles onto the separation column (DB-5ms UI, 30 m × 0.25 mm ID, 0.25 µm film thickness, Agilent Technologies Böblingen, Germany). Further details on GC oven and MSD settings are given by Haberstroh et al. (2018). To quantify specific compounds (i.e., main monoterpenes including trans-β-ocimene), we regularly analyzed calibration curves with authentic standards. We analyzed chromatographic raw data with MassHunter Software (Agilent Technologies Böblingen, Germany). We compared mass spectra with the NIST mass spectral library and the retention times of authentic standards to identify compounds of interest.

10 % of the column effluent was diverted to the MSD by a splitter at the end of the GC column, while the remainder of the sample was transferred to an Isotope Ratio Mass Spectrometer (IRMS; Isoprime precisION, Elementar, Hanau, Germany) via a combustion furnace (GC5 interface, Elementar, Hanau, Germany). The latter was operated at 850 °C and combusted VOCs with CuO to CO_2 and water. After removal of water by a Nafion trap, the CO_2 was directed into the continuous flow IRMS to analyze compound specific $\delta^{13}C$ values. We regularly analyzed octane ($\delta^{13}C$: −31.75 ± 0.01 ‰) and octadecane ($\delta^{13}C$: −32.70 ± 0.01 ‰) (available from Schimmelmann lab, Indiana University, https://arndt.schimmelmann.us/compounds.html) as isotopic reference standards throughout the measurement window. We analyzed raw data with the IonIOS software (Elementar Analysensysteme GmbH, Langenselbold, Germany).

Calculations

For all calculations, we used 15-minute averages from the end of the labeling period (minute 55-70 after label application) to minimize the effects of any disturbance from cutting the leaf and placing it into solution. We calculated the transpiration rate E [mmol $m^{-2}s^{-1}$] and the assimilation rate A [µmol $m^{-2}s^{-1}$] from the concentration of water vapor and CO_2 as in von Caemmerer and Farquahar (1981), using the concentrations from the stable isotope spectrometers (Picarro L2120i and Thermo Delta Ray, respectively). We calculated instantaneous water use efficiency WUE_i [µmol CO_2/mmol H_2O] as the ratio A/E.

We calculated $\delta^{13}C$ values of CO_2 relative to the Vienna Pee Dee Belemnite (VPDB) scale using two internal reference gases ($\delta^{13}C$ values = -9.86 ‰ and -27.8 ‰). We calculated the ^{13}C enrichment of CO_2 ($\varepsilon^{13}C_{CO2}$) leaving the leaf cuvettes following labeling with ^{13}C-pyruvate as

$$\varepsilon^{13}C_{CO2} = \left(\frac{\delta^{13}C_{CO2o}+1000}{\delta^{13}C_{CO2e}+1000} - 1\right), \quad (1)$$

where $\delta^{13}C_{CO2o}$ and $\delta^{13}C_{CO2e}$ are the $\delta^{13}C$ values of CO_2 from the outlet and the entrance of the cuvette, respectively. The term $\varepsilon^{13}C_{CO2}$ is functionally equivalent to $\Delta^{13}C_{CO2}$ as it is frequently used in plant sciences.

We converted $\delta^{13}C$ values to the fraction of ^{13}C ($^{13}F = {}^{13}C/({}^{12}C + {}^{13}C)$) using the definition of $\delta^{13}C$ and the known $^{12}C/^{13}C$ ratio of VPDB (Hayes, 2004). We then used isotopic mass balance to determine the net isotopic effect of photosynthesis and respiration on the ^{13}F value of CO_2 leaving the leaf cuvette, $^{13}F_P$, prior to labeling as:

$$^{13}F_P = \frac{c_e * {}^{13}F_e - c_o * {}^{13}F_o}{c_e - c_o}, \quad (2)$$

where $^{13}F_e$ and $^{13}F_o$ are the ^{13}F values for CO_2 and c_e and c_o are the concentrations of CO_2 at the entrance and outlet of the leaf cuvette, respectively. We averaged $^{13}F_P$ values for all measurements of each species, and assumed that it remained constant throughout the pyruvate

labeling event, because the natural isotopic effect of photosynthesis and respiration on the $\delta^{13}C$ value of the CO_2 leaving the cuvette was relatively small (always less than 10 ‰) relative to the impact of the ^{13}C pyruvate label.

We were then able to calculate the concentration of ^{13}C originating from the pyruvate label, c_l, through isotopic mass balance as:

$$c_I = \frac{c_o*({}^{13}F_o - {}^{13}F_P) + c_e*({}^{13}F_P - {}^{13}F_e)}{F_I}, \quad (3)$$

where the ^{13}F value of the 99 atom % ^{13}C-pyruvate label, F_l, is 0.99. We converted c_l to moles of CO_2 using the ideal gas law and the flow rate of air to the leaf cuvettes, and to grams of CO_2 using the molar mass of CO_2. We then compared this mass to the total mass of ^{13}C taken up from the pyruvate label to determine the percent of pyruvate carbon that was allocated to CO_2.

Volume mixing ratios (VMR, [ppbv]) of VOCs were calculated from counts per second (cps) via mass-dependent transmission of the PTR-TOF-MS, followed by mass scale calibration using PTRwid software (version 003 08-11-2020, (Holzinger, 2015)) following the procedure described by (Holzinger et al., 2019). VOC fluxes, V_l, in [*nmol* $m^{-2}s^{-1}$] were calculated from molar flow u [*nmol* s^{-1}], the leaf area s [m^2], the mixing ratio of the VOC from the outlet of the empty cuvette v_e [*ppbv*], and the mixing ratio of the VOC at the outlet of the leaf cuvette v_o [*ppbv*] as:

$$V_l = \frac{u}{s} * (v_o - v_e). \quad (4)$$

To distinguish VOCs that were synthesized directly from introduced $^{13}C1$- or $^{13}C2$-pyruvate, ${}^{13}V_l$, and VOCs produced only with ^{12}C, ${}^{12}V_l$, we calculated the fraction of the fluxes of mass 69.0683 in relation to mass 70.0719 for isoprene and mass 137.141 in relation to mass 138.145 for monoterpenes. We subsequently subtracted the theoretical value of the contribution of the heavier isotope under natural abundance of ^{13}C (1.1%), ${}^{13}F_{na}$ (isoprene: 5.5%; monoterpenes: 11%) to calculate the excess ^{13}C fraction ${}^{13}F_{Vl}$ in percent:

$$^{13}F_{Vl} = \frac{^{13}V_l}{^{13}V_l + ^{12}V_l} * 100 - {}^{13}F_{na}. \quad (5)$$

To calculate ^{13}C enrichment of individual monoterpenes measured by GC-C-IRMS, we calculated $\varepsilon^{13}C$ values between the $\delta^{13}C$ value of the compound during a specific labeling event ($\delta^{13}C_l$) and the mean $\delta^{13}C$ value of the same compound from unlabeled leaves ($\delta^{13}C_n$) during the same experimental phase (pre-drought or drought):

$$\varepsilon^{13}C = \left(\frac{\delta^{13}C_{CO2o}+1000}{\delta^{13}C_{CO2e}+1000} - 1\right). \quad (6)$$

Statistics

Changes in transpiration, assimilation, VOC fluxes, and ^{13}C-enrichment of CO_2 between pre-drought and drought measurements were compared for each species using Welch's t test. Differences in ^{13}C-enrichment of CO_2 were also assessed using three-way ANOVA followed by Tukey's post hoc test, with species, drought treatment, and position of ^{13}C in the pyruvate label as separate factors. All statistical analyses were performed in Prism (version 9.5.1, GraphPad Software, LLC).

Results

Changes in transpiration, assimilation, and leaf water use efficiency

Transpiration and assimilation rates declined during the drought for all species besides *H. rosa sinensis*, which had low rates in both periods (**Figure 3**). *P. dioica* displayed the highest intraspecies variability in these fluxes, with very high values observed for the leaves of the largest individual, located on the south side of the biosphere, which received more direct sunlight than the individuals on the north side. *C. fairchildiana* displayed the largest relative reductions in transpiration and assimilation, with a relatively greater decline

327 in assimilation, resulting in a significant decrease in water use efficiency (WUE) during the
328 drought (**Figure 3**). Nevertheless, *C. fairchildiana* had the highest WUE of any species in
329 both phases of the experiment (**Figure 3**).
330
331 *VOC fluxes*
332 *C. fairchildiana* had the highest isoprene fluxes of all species under both pre-drought
333 (7 ± 3 nmol m^{-2} s^{-1}) and drought (1.1 ± 0.9 nmol m^{-2} s^{-1}) conditions (**Figure 4**). *P. auritum*
334 had the second highest isoprene fluxes, but these were an order of magnitude lower than
335 those from *C. fairchildiana* (0.1 ± 0.04 nmol m^{-2} s^{-1} under pre-drought conditions and $1*10^{-4}$
336 ± $9*10^{-5}$ nmol m^{-2} s^{-1} under drought conditions; **Figure 4**). Isoprene emissions from *H. rosa*
337 *sinensis* and *P. dioica* were only present in trace amounts (not shown). Between the pre-
338 drought and drought, isoprene emissions only declined significantly for *P. auritum* ($p < 0.05$),
339 but there were declining tendencies in emissions for *C. fairchildiana* as well (**Figure 4**).
340 Monoterpene emissions were also at least an order of magnitude higher from *C.*
341 *fairchildiana* than any other species (**Figure 4**), but were two orders of magnitude lower than
342 its isoprene emissions. Monoterpene emissions declined under drought (**Figure 4**), but not
343 significantly. Analysis of cartridge samples by GC-MS (which is able to chromatographically
344 resolve different monoterpenes) indicated that α-pinene, β-pinene, 3-carene, limonene, and
345 trans-β-ocimene were the most abundant monoterpenes emitted by *C. fairchildiana* (**Table**
346 **1**). Fluxes of most of these compounds declined with drought, but trans-β-ocimene emissions
347 increased by a factor of four (**Table 1**).
348
349 *^{13}C-enrichment of CO_2 from pyruvate*
350 All studied plants in Biosphere 2 displayed the expected pattern of more ^{13}C-enriched
351 CO_2 following labeling with ^{13}C1-pyruvate than with ^{13}C2-pyruvate (**Figures 5, 6**). For most

352 species, the difference in the percentage of ^{13}C from $^{13}C1$-pyruvate that was converted to CO_2
353 was significantly higher than the percentage of ^{13}C from $^{13}C2$-pyruvate that was converted to
354 CO_2 during pre-drought (**Figure 5**). However, this difference was not significant for *C.*
355 *fairchildiana* at any time, nor for *P. auritum* during drought. As much as ~10 % of the total
356 ^{13}C from the $^{13}C1$-pyruvate was decarboxlated (or released) in the light during the 80 minutes
357 of our measurements, in contrast to less than 1.5 % of the total ^{13}C taken up from the $^{13}C2$-
358 pyruvate (**Figure 5**). However, the magnitude of this difference tended to be less pronounced
359 for *C. fairchildiana* and *P. auritum* than for *H. rosa sinensis* and *P. dioica* (**Figures 5, 6)**.
360 This difference is apparent by plotting the $\varepsilon^{13}C_{CO2}$ (i.e., the change in $\delta^{13}C$ values of CO_2 due
361 to labeling) values from $^{13}C1$-pyruvate labeling relative to those from $^{13}C2$-pyruvate labeling,
362 where the values for *C. fairchildiana* and *P. auritum* plot much closer to the 1:1 line than the
363 other species do (**Figure 6**). During drought, the $\varepsilon^{13}C_{CO2}$ values during labeling with both
364 pyruvate labels tended to decline for both *C. fairchildiana* and *P. auritum*, while for *P. dioica*
365 they only tended to decline for labeling with $^{13}C1$-pyruvate and for *H. rosa sinensis* they did
366 not change (**Figure 6**).
367
368 *^{13}C-enrichment of VOCs following pyruvate labeling*
369 Emissions of isoprene and monoterpenes in *C. fairchildiana* were clearly enriched in
370 ^{13}C following the ^{13}C-pyruvate labeling during both pre-drought and drought conditions. For
371 isoprene, up to 15 % of the isoprene flux was labeled with ^{13}C above the natural background
372 level (**Figure 7a**), indicating that a sizable amount of isoprene was freshly synthesized from
373 pyruvate. During pre-drought conditions, there was no significant difference in the
374 incorporation of ^{13}C into isoprene fluxes from the $^{13}C1$- and $^{13}C2$-pyruvate labels (**Figure**
375 **7a**). Similarly, under drought, there was no significant difference in ^{13}C-incorporation

between both labels. However, ^{13}C-incorporation in isoprene increased under drought, though this was significant only for $^{13}C1$-labeling (**Figure 7a**).

Of the monoterpenes emitted from *C. fairchildiana*, only trans-β-ocimene was strongly enriched in ^{13}C following labeling by either type of pyruvate, with relatively higher ^{13}C enrichment from $^{13}C2$-pyruvate than from $^{13}C1$ (**Figure 7b**). Under drought, trans-β-ocimene ^{13}C enrichment was similar from both pyruvate labels, with a tendency to decline under drought (**Figure 7b**).

Discussion

We used position-specific ^{13}C-pyruvate labeling to investigate leaf level metabolic processes before and during an experimental drought in the Biosphere 2 tropical rainforest, with an emphasis on understanding changes in allocation of the central metabolite pyruvate into CO_2 and VOCs in the context of overall drought responses. We focused on four tropical species with clear differences in their drought responses at both the level of individual leaves (**Figure 3**) and in terms of whole plant responses such as leaf water potential, sap flow, and leaf shedding (Werner et al., 2021). In the following discussion, we evaluate our three hypotheses about allocation of ^{13}C from pyruvate into CO_2 and VOCs and place these results into the context of the plants' overall drought responses.

Drought response of $^{13}CO_2$ production from pyruvate is primarily species dependent

Our first hypothesis, that large reductions in assimilation and transpiration in drought-sensitive plants would also produce less day-time CO_2 emission from pyruvate, was partially supported. While the drought-tolerant species, *H. rosa sinensis* and *P. dioica,* did not show any decline in the percentage of pyruvate that was converted to CO_2, the drought-sensitive *P. auritum* did indeed produce less ^{13}C-enriched CO_2 during drought than before (**Figure 5**).

401 Surprisingly, *C. fairchildiana,* the species displaying the overall strongest drought response,
402 did not show such a decline in pyruvate use for $^{13}CO_2$ production. Overall pyruvate use
403 differed significantly between *C. fairchildiana* and the other three species (**Figure 5**),
404 indicating fundamental differences in the general use of the central metabolite pyruvate in *C.*
405 *fairchildiana*, which will be discussed in more detail below.

406 Our second hypothesis, that the majority of cytosolic pyruvate would be used for non-
407 mitochondrial processes under control conditions, but converge with use in the TCA cycle in
408 accordance to drought response, was also partially supported. In the drought-tolerant species
409 *P. dioica* and *H. rosa sinensis*, cytosolic pyruvate was much more likely to be used for non-
410 mitochondrial anabolic processes than within the TCA cycle before and during drought
411 (**Figure 5, 6**). However, the difference in relative allocation of pyruvate became smaller in *H.*
412 *rosa sinensis* during drought, mainly because of increased cytosolic pyruvate use within the
413 TCA cycle, as evidenced by increased emissions of $^{13}CO_2$ following labeling with ^{13}C2-
414 pyruvate (**Figure 5, 6**). This shift towards more daytime TCA activity may have indicated an
415 early drought response in these mostly light-limited plants. On the other hand, for the
416 drought-sensitive *P. auritum* pyruvate consumption declined for all CO_2 generating
417 processes, indicating an overall slowdown of multiple metabolic pathways with drought.
418 While drought-stressed *P. auritum* plants still tended to produce more $^{13}CO_2$ from ^{13}C1-
419 pyruvate than from ^{13}C2-pyruvate, this difference was no longer significant (**Figure 5, 6**).

420 Contrary to expectations based on multiple growth-chamber experiments with
421 unstressed plants (e.g., Tcherkez et al., 2008; Priault et al., 2009; Fasbender et al., 2018;
422 Yáñez-Serrano et al., 2019; Werner et al., 2020; Kreuzwieser et al., 2021), the percentage of
423 $^{13}CO_2$ that was produced from ^{13}C1-pyruvate by *C. fairchildiana* was not significantly higher
424 than that produced from ^{13}C2-pyruvate (**Figure 5**). Additionally, the percentage of pyruvate
425 allocated to CO_2-producing pathways did not change appreciably with drought. Overall, these

426 results suggest that *C. fairchildiana* uses pyruvate in fundamentally different ways than the
427 plants in earlier studies, and that its pyruvate metabolism is minimally affected by drought
428 despite its large drought responses in terms of transpiration and assimilation (**Figure 3**), as
429 well as leaf water potential, sap flow, and leaf shedding (Werner et al., 2021).
430
431 *Potential sinks for cytosolic pyruvate in C. fairchildiana*
432 Overall, *C. fairchildiana* decarboxylates significantly lower amounts of cytosolic
433 pyruvate than other plant species, even when it becomes increasingly carbon limited due to
434 strongly reduced assimilation under drought, raising the question how pyruvate is used by this
435 species instead. Here we explore two likely metabolic pathways of use of pyruvate in *C.*
436 *fairchildiana* that would explain the allocation of all three carbons to biosynthetic products,
437 rather than CO_2: anaplerotic recapture of decarboxylated C feeding an enhanced, non-cyclic
438 TCA flux that supplies amino acid precursors, and incorporation of the whole pyruvate
439 molecule into isoprenoids via glyceraldehyde 3-phosphate (GA-3-P).
440 In the light, the reactions of TCA metabolism are better conceived of as a non-cyclic
441 flux rather than a cycle (Sweetlove et al., 2010). While the traditional nocturnal mode of the
442 TCA cycle produces energy and consumes acetyl-CoA produced from pyruvate, this pathway
443 can serve many other functions in plants during the day. In particular, citrate and 2-oxoglutarate
444 produced by TCA metabolism can be exported and form the carbon backbones of amino acids
445 such as glutamate and glutamine (Hanning and Heldt, 1993; Tcherkez et al., 2009). Additional
446 sources of carbon besides acetyl-CoA are required to sustain this carbon flux from the TCA
447 cycle, and can be provided anaplerotically by oxaloacetate (OAA) produced from
448 phospho*enol*pyruvate (PEP) and CO_2 (Tcherkez et al., 2009; Sweetlove et al., 2013) (**Figure**
449 **2**). We hypothesize that the required CO_2 for OAA production is at least partially directly
450 supplied by the decarboxylation of pyruvate to form acetyl-CoA. This would explain the

451 relatively low amount of $^{13}CO_2$ produced from the $^{13}C1$-pyruvate label that we observed.
452 Indeed, *C. fairchildiana* may have a greater demand for carbon backbones for amino acids than
453 the other species, since it is a legume and therefore has higher nitrogen content than the other
454 taxa. A similar reduction in $^{13}CO_2$ production from $^{13}C1$-pyruvate has also been observed for
455 soil microbial communities when they are provided with succinate or with leaves from
456 legumes, both of which increase nitrogen availability, making an anaplerotically fed open flux
457 mode of the TCA metabolism more favorable (Dijkstra et al., 2011).

458 Biosynthesis of isoprenoids could be another significant sink for cytosolic pyruvate in
459 *C. fairchildiana*, which was the only strong isoprenoid emitter among the species we analyzed
460 in B2 rainforest (**Figure 4**). Since we observed no differences between $^{13}C1$- and $^{13}C2$-pyruvate
461 incorporation into isoprene (**Figure 7**), the primary route by which pyruvate appears to have
462 been incorporated into isoprene in *C. fairchildiana* was via GA-3-P, which conserves all three
463 carbon atoms from the original pyruvate atom, and not via decarboxylated pyruvate (as
464 reported by Yáñez-Serrano et al. 2019; Werner et al. 2020; Kreuzwieser et al., 2021), which
465 would result in greater ^{13}C-enrichment following labeling with $^{13}C2$-pyruvate compared to
466 $^{13}C1$-pyruvate (**Figure 2**). A significant use of cytosolic pyruvate for isoprenoid biosynthesis
467 via GA-3-P would account for the observed similar production of $^{13}CO_2$ from both label types
468 and has previously been observed for some MEP-derived isoprenoids (Ladd et al., 2021).
469 Consequently, these patterns could also partially explain the significant differences in $^{13}CO_2$
470 production from labeled pyruvate that we observed between *C. fairchildiana* and the other three
471 species.

472

473 *Different patterns of ^{13}C incorporation into isoprene and monoterpenes in C. fairchildiana*

474 We were only able to evaluate our third hypothesis, that the proportion of isoprenoids
475 synthesized from cytosolic pyruvate would increase under drought, for *C. fairchildiana*, which

476 was the only species that emitted sufficiently high enough quantities of isoprenoids for isotopic
477 analyses. In *C. fairchildiana*, this hypothesis was supported for isoprene, as the ^{13}C-enrichment
478 of emitted isoprene following ^{13}C-pyruvate labeling increased under drought (**Figure 7**), even
479 while overall isoprene emissions declined (**Figure 4**). These results indicate that synthesis of
480 isoprene from primary photosynthate by *C. fairchildiana* declined under drought as
481 assimilation also declined, resulting in an increased proportion of the remaining isoprene flux
482 being dependent on cytosolic pyruvate (**Figure 8, step 2-4**) similar to what has been observed
483 for heat-stressed plants in growth chambers (Yáñez-Serrano et al., 2019).
484 Surprisingly, increased ^{13}C-enrichment of monoterpenes following ^{13}C-pyruvate
485 labeling did not increase under drought (**Figure 7**), contradicting our expectations that
486 isoprene and monoterpenes would behave similarly to each other since they are both derived
487 from IPP and its isomer dimethylallyl pyrophosphate (DMAPP) produced in the MEP
488 pathway (**Figure 2, step 4**). IPP and DMAPP are also produced in the cytosolic MVA
489 pathway, where pyruvate is incorporated only via acetyl-CoA, with its C1 position being
490 decarboxylated (**Figure 2, step 5**). Possibly, geranyl pyrophosphate (GPP), an intermediate
491 between IPP and monoterpenes that is produced in both the MVA and MEP pathways
492 (Bouvier et al., 2001; Schmidt and Gershenzon, 2007; Zulak et al., 2010), is produced from
493 cytosolic pyruvate and transported into the plastid to supply monoterpene synthesis, but not
494 isoprene synthesis (Bick and Lange, 2003; Gutensohn et al., 2012) during pre-drought
495 conditions. This would explain why pre-drought trans-β-ocimene tended to become more
496 ^{13}C-enriched following labeling with ^{13}C2-pyruvate than with ^{13}C1-pyruvate while the
497 relative ^{13}C-enrichment was similar for isoprene from both labels (**Figure 8**). Alternatively,
498 the same pattern could be observed if trans-β-ocimene was synthesized as a byproduct of
499 sesquiterpene synthesis (Davidovich-Rikanati et al. 2008; Gutensohn et al. 2013) or via
500 enzymes of the Nudix hydrolase family (Magnard et al., 2015; Liu et al., 2018) in the cytosol.

501 However, these processes are unlikely to drive the observed patterns as *C. fairchildiana* did
502 not emit any sesquiterpenes and the presence of monoterpene synthesis via Nudix hydrolases
503 in vegetative tissue has yet to be shown. We therefore consider an MVA-derived GPP
504 contribution to pre-drought monoterpenes to be a more likely explanation for the different
505 patterns of ^{13}C incorporation into isoprene and trans-β-ocimene.

506 During drought, trans-β-ocimene synthesis from MVA derived GPP apparently
507 declined or even completely ceased (**Figure 8, step 5**), as the ^{13}C-enrichment of β-ocimene
508 was similar from both $^{13}C1$- and $^{13}C2$-pyruvate, similar to isoprene (**Figure 7**). In contrast to
509 isoprene, ^{13}C enrichment of trans-β-ocimene tendentially declined with drought, indicating
510 less reliance on cytosolic pyruvate for the synthesis of these compounds, even as cytosolic
511 pyruvate apparently became more important for supporting the isoprene flux (**Figure 7**). The
512 differing patterns for ^{13}C incorporation into isoprene and trans-β-ocimene emissions are
513 intriguing and further experiments are needed to fully disentangle the mechanisms
514 responsible for the observed patterns.

515

516 **Conclusions**

517 Biochemical experiments including position-specific ^{13}C-labeling are usually
518 conducted under highly-controlled laboratory conditions on small saplings. Here, we applied
519 this approach to mature plants in a near-natural ecosystem. Three of the four species we
520 investigated generally conformed to expectations about the relationship between functional
521 drought responses and use of cytosolic pyruvate. Specifically, daytime production of CO_2
522 from pyruvate declined more as drought stress increased, more daytime CO_2 was produced
523 from non-mitochondrial biosynthetic pathways than from TCA metabolism, and there was
524 convergence between these two sources of CO_2 as drought stress increased. However, we
525 observed strikingly different and novel results from *C. fairchildiana*, a legume tree that is

526 also a strong isoprenoid emitter. In particular, CO_2 production from pyruvate was relatively
527 low in this species during both pre-drought and drought conditions, and CO_2 production from
528 the C1 position of pyruvate was not significantly higher than from the C2 position. This
529 suggests that *C. fairchildiana* efficiently incorporates all three carbon atoms from pyruvate
530 into metabolic products including amino acids and isoprenoids. The patterns of ^{13}C
531 incorporation into different isoprenoids emitted by *C. fairchildiana* also suggests that
532 crosstalk between the cytosolic MVA and the plastidic MEP pathways for isoprenoid
533 synthesis is important for monoterpene synthesis, but not isoprene synthesis, and that this
534 metabolic crosstalk declines with drought. *C. fairchildiana* over-proportionally contributed to
535 overall isoprene emissions and GPP of the whole ecosystem before drought and played a
536 major role in the decline of these fluxes during drought (Werner et al., 2021). Identifying and
537 understanding metabolic adjustments of drought-sensitive plant species like *C. fairchildiana*
538 that significantly contribute to ecosystem VOC emissions in natural tropical ecosystems
539 could therefore help to improve current attempts to model drought impacts on VOC
540 production in tropical rainforests, which are the major source (>80 %) of global isoprene
541 emissions (Sindelarova et al., 2014).
542
543 **Supplementary data:**

Table S1: Leaf temperatures inside enclosed leaf cuvettes during the experiments in comparison to ambient daytime temperature ranges inside the Biosphere 2 tropical rainforest.

544
545 **Conflict of Interest:** none declared
546

Funding: This research was funded by the European Research Council (ERC consolidator grant 647008 to CW) and financial support from the Philecology Foundation to Biosphere 2 (obtained by LKM).

Acknowledgements: The study took place within the context of the B2WALD campaign, and was supported by the wider efforts of the entire B2WALD team, as described on the team contribution list (https://doi.org/10.25422/azu.data.14632662). We are particularly grateful to Michael Burman, Marissa Clover, Sydney Kerman, and Luke Miller for their assistance with leaf labeling in the forest canopy.

Author Contributions: Conceptualization (CW, SNL, LED); Data curation (LED, IB, JVH, LKM), Formal analysis (LED, SNL, JK, IB, AK, JVH, GP); Funding acquisition (CW, LKM); Investigation (SNL, LED, IB, JD, JVH, GP, JI, CW, AK); Methodology (CW, JK, IB, LED, SNL); Project administration (CW, SNL); Resources (CW, JVH, LKM); Supervision (CW, LKM, SNL); Validation (AK, CW, IB, LED, SNL); Visualization (LED, SNL); Writing – original draft (SNL, LED); Writing – review & editing: all.

References:

Atkinson R, Arey J. 2003. Gas-phase tropospheric chemistry of biogenic volatile organic compounds: a review. Atmospheric Environment 37, 197-219.

Bick JA, Lange BM. 2003. Metabolic cross talk between cytosolic and plastidial pathways of isoprenoid biosynthesis: unidirectional transport of intermediates across the chloroplast envelope membrane. Archives of Biochemistry and Biophysics 415, 146-154.

Bouvier F, Suire C, D'Harlingue A, Backhaus RA, Camara B. 2001. Molecular cloning of geranyl diphosphate synthase and compartmentation of monoterpene synthesis in plant cells. The Plant Journal 24, 241-252.

Claeys M, Graham B, Vas G, Wang W, Vermeylen R, Pashynska V, Cafmeyer J, et al. 2004. Formation of secondary organic aerosols through photooxidation of isoprene. Science 303, 1173-1176.

Davidovich-Rikanati R, Lewinsohn E, Bar E, Iijima Y, Picherksy E, Sitrit Y. 2008. Overexpression of the lemon basil α-zingiberene synthase gene increases both mono- and sesquiterpene contents in tomato fruit. The Plant Journal 56, 228-238.

Dijkstra P, Blankinship JC, Selmants PC, Hart SC, Koch GW, Schwartz E, Hungate, BA. 2011. Probing carbon flux patterns through soil microbial metabolic networks using parallel position-specific tracer labeling. Soil Biology & Biochemistry 43, 126-132.

Douville H, Raghavan K, Renwick J, Allan RP, Arias PA, Barlow M, Cerezo-Mota, et al. 2021. Water Cycle Changes. In Masson-Delmotte V, Zhai P, Pirani A, Connors SL, Pean C, Berger S, Caud N, et al., eds. Climate Change 2021: The Physical Science Basis. Contribution of Working Group I to the Sixth Assessment Report of the Intergovernmental Panel on Climate Change. Cambridge University Press, Cambridge, United Kingdom and New York, NY, USA, 1055-1210.

Evaristo J, Kim M, van Haren J, Pangle LA, Harman CJ, Troch PA, McDonnell JJ. 2019. Characterizing the fluxes and age distribution of soil water, plant water, and deep percolation in a model tropical ecosystem. Water Resources Research 55, 3307-3327.

Fasbender L, Yáñez-Serrano AM, Kreuzwieser J, Dubbert D, Werner, C. 2018. Real-time carbon allocation into biogenic volatile organic compounds (BVOCs) and respiratory carbon dioxide (CO_2) traced by PTR-TOF-MS, $^{13}CO_2$ laser spectroscopy and ^{13}C-pyruvate labelling. PLOS One 13, e0204398.

Graus M, Schnitzler J-P, Hansel A, Cojocariu C, Rennenberg H, Wisthaler A, et al. 2004 Transient release of oxygenated volatile organic compounds during light-dark transitions in grey poplar leaves. Plant Physiology 135, 1967-1975.

Guenther A, Karl T, Harley P, Wiedinmyer C, Palmer PI, Geron C. 2006. Estimates of global terrestrial isoprene emissions using MEGAN (Model of Emissions of Gases and Aerosols from Nature). Atmospheric Chemistry and Physics 6, 3181-3210.

Gutensohn M, Nagegowda DN, Dudareva N. 2012. Involvement of compartmentalization in monoterpene and sesquiterpene biosynthesis in plants. In: Bach TJ, Rohmer M, eds.

Isoprenoid Synthesis in Plants and Microorganisms. Springer Science and Business Media, New York, NY, USA, 155-169.

Gutensohn M, Orlova I, Nguyen TTH, Davidovich-Rikanati R, Ferruzzi MG, Sitrit Y, Lewinsohn E, Pichersky E, Dudareva N. 2013. Cytosolic moterpene biosynthesis is supported by plastid-generated geranyl diphosphate substrate in transgenic tomato fruits. The Plant Journal 75, 351-363.

Haberstroh S, Kreuzwieser J, Lobo-do-Vale R, Caldeira MC, Werner C. 2018. Terpenoid emissions of two Mediterranean woody species in response to drought stress. Frontiers in Plant Science 9, 1071. doi: 10.3389/fpls.2018.01071

Hanning I, Heldt, HW. 1993. On the function of mitochondrial metabolism during photosynthesis in spinach (*Spinacia oleracea* L.) leaves (partitioning between respiration and export of redox equivalents and precursors for nitrate assimilation products). Plant physiology 103, 1147-1154.

Hayes JM. 2004. An introduction to isotopic calculations. Woods Hole Oceanographic Institution, Woods Hole, MA, 2543.

Holzinger R. 2015. PTRwid: A new widget tool for processing PTR-TOF-MS data. Atmospheric Measurement Techniques 8, 3903-3922.

Holzinger R, W. Acton JF, Bloss WJ, Breitenlechner M, Crilley LR, Dusanter S, Gonin M, et al. 2019. Validity and limitations of simple reaction kinetics to calculate concentrations of organic compounds from ion counts in PTR-MS. Atmospheric measurement techniques 12, 6193-6208.

Hubau W, Lewis SL, Phillips OL, et al. 2020. Asynchronous carbon sink saturation in African and Amazonian tropical forests. Nature 579, 80-87.

Jardine KJ, Sommer ED, Saleska SR, Huxman TE, Harley PC, Abrell L. 2010. Gas phase measurements of pyruvic acid and its volatile metabolites. Environmental Science & Technology 44, 2454-2460.

Jardine K, Wegener F, Abrell L, van Haren J, Werner C. 2014. Phytogenic biosynthesis and emission of methyl acetate. Plant, Cell & Environment 37, 414–424.

Kreuzwieser J, Meischner M, Grün M, Yáñez-Serrano AM, Fasbender L, Werner C. 2021. Drought affects carbon partitioning into volatile organic compound biosynthesis in Scots pine needles. New Phytologist 232, 1930-1943.

Kübert A, Dubbert M, Bamberger I, Kühnhammer K, Beyer M, van Haren J, Bailey K, et al. 2023. Tracing plant source water dynamics during drought by continuous transpiration measurements: an *in-situ* stable isotope approach. Plant, Cell & Environment 46, 133-149.

Ladd SN, Nelson DB, Bamberger I, Daber LE, Kreuzwieser J, Kahmen A, Werner C. 2021. Metabolic exchange between pathways for isoprenoid synthesis and implications for biosynthetic hydrogen isotope fractionation. New Phytologist 231, 1708-1719.

Lelieveld J, Butler TM, Crowley JN, Dillon TJ, Fischer H, Ganzeveld L, Harder H, et al. 2008. Atmospheric oxidation capacity sustained by a tropical forest. Nature 452, 737-740.

Lichtenthaler HK, Rohmer M, Schwender J. 1997. Two independent biochemical pathways for isopentenyl diphosphate and isoprenoid biosynthesis in higher plants. Physiologia Plantarum 101, 643-652.

Liu J, Guan Z, Liu H, Qi L, Zhang D, Zou T, Yin P. 2018. Structural insights into the substrate recognition mechanism of *Arabidopsis* GPP-bound NUDX1 for noncanonical monoterpene biosynthesis. Molecular Plant 11, 218-221.

Lloyd, J, Farquhar, GD. 2008. Effects of rising temperatures and [CO_2] on the physiology of tropical forest trees. Philosophical Transactions of the Royal Society B 363, 1811-1817.

Magnard J-L, Roccia A, Caissard J-C, Vergne P, Sun P, Hecquet R, Dubois A, et al. 2015. Biosynthesis of monoterpene scent compounds in roses. Science 349, 81-83.

Massé G, Belt ST, Rowland SJ, Rohmer M. 2004. Isoprenoid biosynthesis in the diatoms *Rhizolenia setigera* (Brightwell) and *Haslea ostrearia* (Simonsen). Proceedings of the National Academy of Sciences of the United States of America 101, 4413-4418.

Mitchard ETA. 2018. The tropical forest carbon cycle and climate change. Nature 559, 537-534.

Peñuelas J, Llusià J. 2003. BVOCs: plant defense against climate warming? Trends in Plant Science 8, 105-109.

Pegoraro, E, Rey ANA, Abrell L, Van Haren J, Lin G. 2006. Drought effect on isoprene production and consumption in Biosphere 2 tropical rainforest." Global Change Biology 12, 456-469.

Priault P, Wegener F, Werner C. 2009. Pronounced differences in diurnal variation of carbon isotope composition of leaf respired CO_2 among functional groups. New Phytologist, 181, 400-412.

Rascher U, Bobich EG, Lin GH, et al. 2004. Functional diversity of photosynthesis during drought in a model tropical rainforest - the contributions of leaf area, photosynthetic electron transport and stomatal conductance to reduction in net ecosystem carbon exchange. Plant, Cell & Environment 27, 1239-1256.

Rosolem R, Shuttleworth WJ, Zeng X, Saleska SR, Huxman TE. 2010. Land surface modeling inside the Biosphere 2 tropical rain forest biome. Journal of Geophysical Research Atmospheres 115, doi: 10.1029/2010JG001443

Schmitt A, Gershenzon J. 2007. Cloning and characterization of isoprenyl diphosphate synthases with farnesyl diphosphate and geranylgeranyl diphosphate synthase activity from Norway spruce (*Picea abies*) and their relation to induced oleoresin formation. Phytochemistry 68, 2649-2659.

Schnitzler J-P, Graus M, Kreuzwieser J, Heizmann U, Rennenberg H, Wisthaler A, et al. 2004. Contribution of different carbon sources to isoprene biosynthesis in poplar leaves. Plant Physiology 135, 152-160.

Schuhr CA, Radykewicz T, Sagner S, Latzel C, Zenk MH, Arigoni D, Bacher A, Rohdich F, Eisenreich W. 2003. Quantitative assessment of crosstalk between the two isoprenoid biosynthesis pathways in plants by NMR spectroscopy. Phytochemistry Reviews 2, 3-16.

Schwender J, Seemann M, Lichtenthaler HK, Rohmer M. 1996. Biosynthesis of isoprenoids (carotenoids, sterols, prenyl side-chains of chlorophylls and plastoquinone) via a novel pyruvate/glyceraldehyde 3-phosphate non-mevalonate pathway in the green alga *Scenedesmus obliquus*. Biochemistry Journal 316, 73-80.

Sindelarova K, Granier C, Bouarar I, Guenther A, Tilmes S, Stavrakou T, Müller JF, et al. 2014. Global data set of biogenic VOC emissions calculated by the MEGAN model over the last 30 years. Atmospheric Chemistry and Physics 14, 9317-9341.

Sweetlove LJ, Beard KFM, Nunes-Nesi A, Fernie AR, Ratcliffe RG. 2010. Not just a circle: flux modes in the plant TCA cycle. Trends in plant science 15, 462-470.

Sweetlove LJ, Williams TCR, Cheung MCY, Ratcliffe RG. 2013. Modelling metabolic CO_2 evolution – a fresh perspective on respiration. Plant, Cell & Environment 36, 1631-1640.

Tcherkez G, Cornic G, Bligny R, Gout E, Ghashghaie J. 2005. In vivo respiratory metabolism of illuminated leaves. Plant Physiology 138, 1596-1606.

Tcherkez G, Bligny R, Gout E, Mahé A, Hodges M, Cornic G. 2008. Respiratory metabolism of illuminated leaves de- pends on CO2 and O2 conditions. Proceedings of the National Academy of Sciences of the United States of America 105, 797-802.

Tcherkez G, Mahé A, Cauthier P, Mauve C, Gout E, Bligny R, Cornic G, Hodges M. 2009. In folio respiratory fluxomics revealed by ^{13}C isotopic labeling and H/D isotope effects highlight the noncyclic nature of the the tricarboxylic acid "cycle" in illuminated leaves. Plant Physiology 151, 620-630.

Tcherkez G, Boex-Fontvieille E, Mahé A, Hodges M. 2012. Respiratory carbon fluxes in leaves. Current Opinion in Plant Biology 15 308-314.

von Caemmerer S, Farquhar GD. 1981. Some relationships between the biochemistry of photosynthesis and the gas exchange of leaves. Planta 153, 376-387.

Werner C, Wegener F, Unger S, Nogués S, Priault P. 2009. Short-term dynamics of isotopic composition of leaf respired CO_2 upon darkening: measurements and implications. Rapid Communications in Mass Spectrometry 23, 2428-2438.

Werner C, Fasbender L, Romek KM, Yáñez-Serrano AM, Kreuzwieser, J. 2020. Heat waves change plant carbon allocation among primary and secondary metabolism altering CO_2 assimilation, respiration, and VOC emissions. Frontiers in Plant Science 11, 1242.

Werner C, Meredith LK, Ladd SN, Ingrisch J, Kübert A, van Haren J, et al. 2021. Ecosystem fluxes during drought and recovery in an experimental forest. Science 374, 1514-1518.

Yáñez-Serrano AM, Mahlau L, Fasbender L, Byron J, Williams J, Kreuzwieser J, Werner C. 2019. Heat stress increases the use of cytosolic pyruvate for isoprene biosynthesis. Journal of Experimental Botany 70, 5827-5838.

Zulak KG, Bohlmann, J. 2010. Terpenoid biosynthesis and specialized vascular cells of conifer defense. Journal of Integrative Plant Biology 52, 86-97.

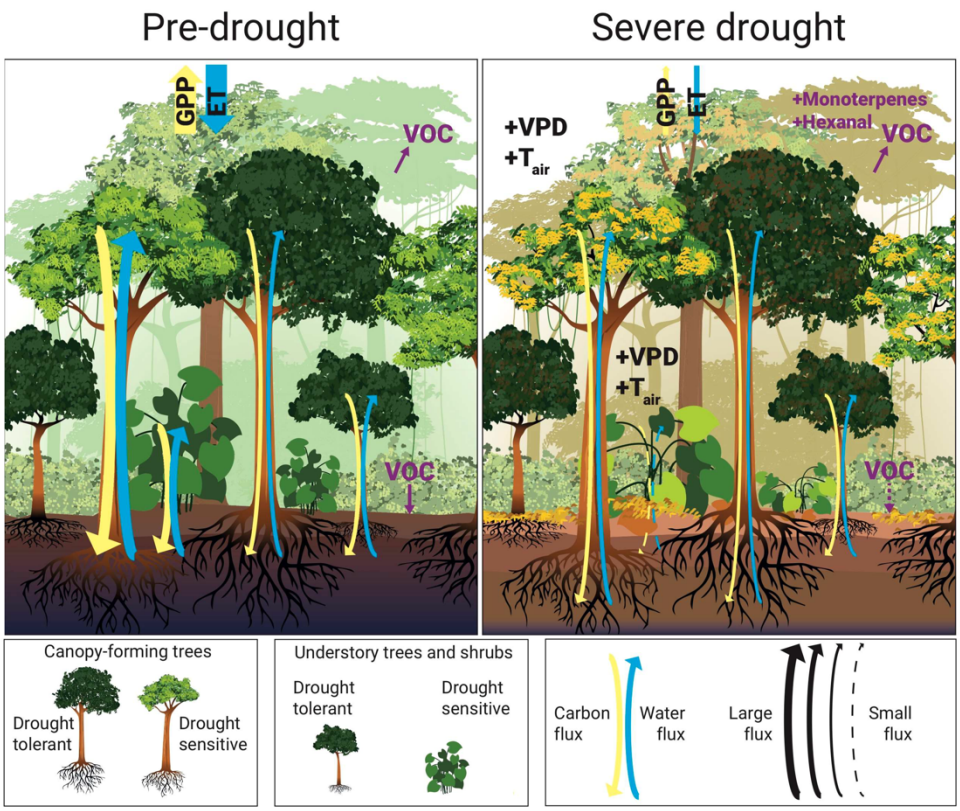

Figure 1: Schematic representation of drought-responses by four plant functional groups identified in the B2 WALD drought, modified from Werner et al., 2021. Drought-sensitive canopy trees were responsible for the majority of ecosystem fluxes before the drought, but rapidly dropped leaves and reduced transpiration demand as upper soil layers dried. Their drought-tolerant counterparts never moved water through their stems as quickly, but had much smaller reductions in activity and leaf water potential in response to drought. Meanwhile, in the understory, drought tolerance was largely driven by microclimate variability, with shaded plants having low fluxes of carbon and water throughout the study period that did not change with drought and were most likely determined by limited light availability. Understory plants in locations with more light availability, either from canopy gaps or windows, were much more sensitive to drought and were the most stressed plants by the end of the experimental drought.

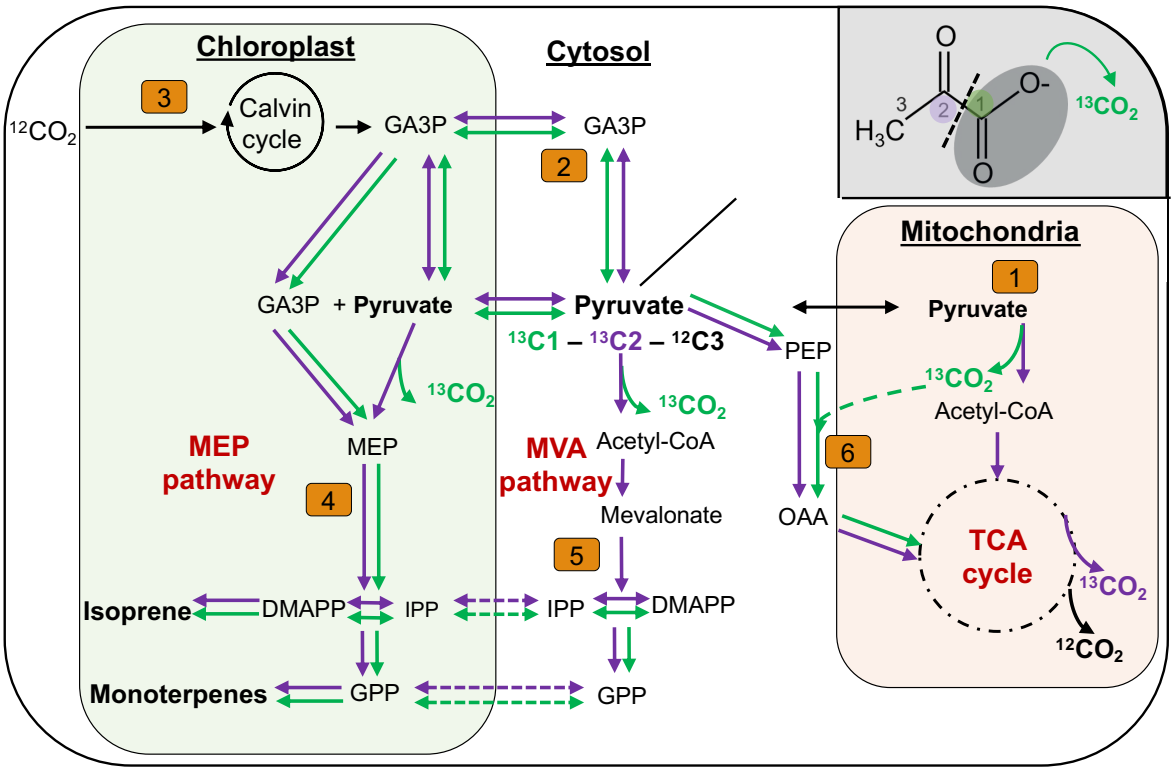

Figure 2: Schematic representation of important processes for the synthesis of isoprenoids and production of CO_2 within plant cells, with several intermediate steps removed for clarity. Green arrows represent possible movement of carbon from the C1 position of pyruvate and purple arrows represent movement of carbon from the C2 position of pyruvate. Numbers represent the relevant steps discussed. 1: Transport of pyruvate into mitochondria, followed by initial decarboxylation of the C1-position and entrance into the TCA-cycle. 2: Conversion of pyruvate to GA-3-P and transport into the chloroplast. Pyruvate might also be transported directly to the chloroplast. All carbon positions of pyruvate remain in both cases. 3: Entrance of CO_2 into the Calvin cycle and addition of GA-3-P and other assimilation products into the metabolic pool of the chloroplast. 4: Initial reaction of pyruvate and GA-3-P to form DMAPP and IPP via MEP pathway, followed by reaction of two DMAPP/IPP molecules to produce GPP. As GA-3-P is not decarboxylated in this reaction, all carbon positions of the converted GA-3-P remain in the produced isoprene and monoterpenes. Pyruvate on the other hand is decarboxylated, resulting in only the C2-position remaining in these products 5: Entrance of pyruvate into MVA pathway and initial decarboxylation of the C1-position of pyruvate to form DMAPP, IPP and subsequently GPP in the cytosol. After transport of these metabolites incorporating the $^{13}C2$-label into the chloroplast, DMAPP and IPP can either enter isoprene or monoterpene synthesis, while GPP is used to synthesize monoterpenes. 6: Anaplerotic replenishment of OAA to the TCA cycle from PEP and CO_2, which can support the production of carbon backbones for N-containing compounds. Abbreviations: TCA, tricarboxlic acid; GA-3-P, glyceraldehyde 3-phosphate; DMAPP Dimethylallyl pyrophosphate; IPP, isopentenyl pyrophosphate; MEP, methylerythritol phosphate; GPP, geranyl pyrophosphate; MVA, mevalonic acid; PEP, phospho*enol*pyruvate; OAA, oxaloacetate.

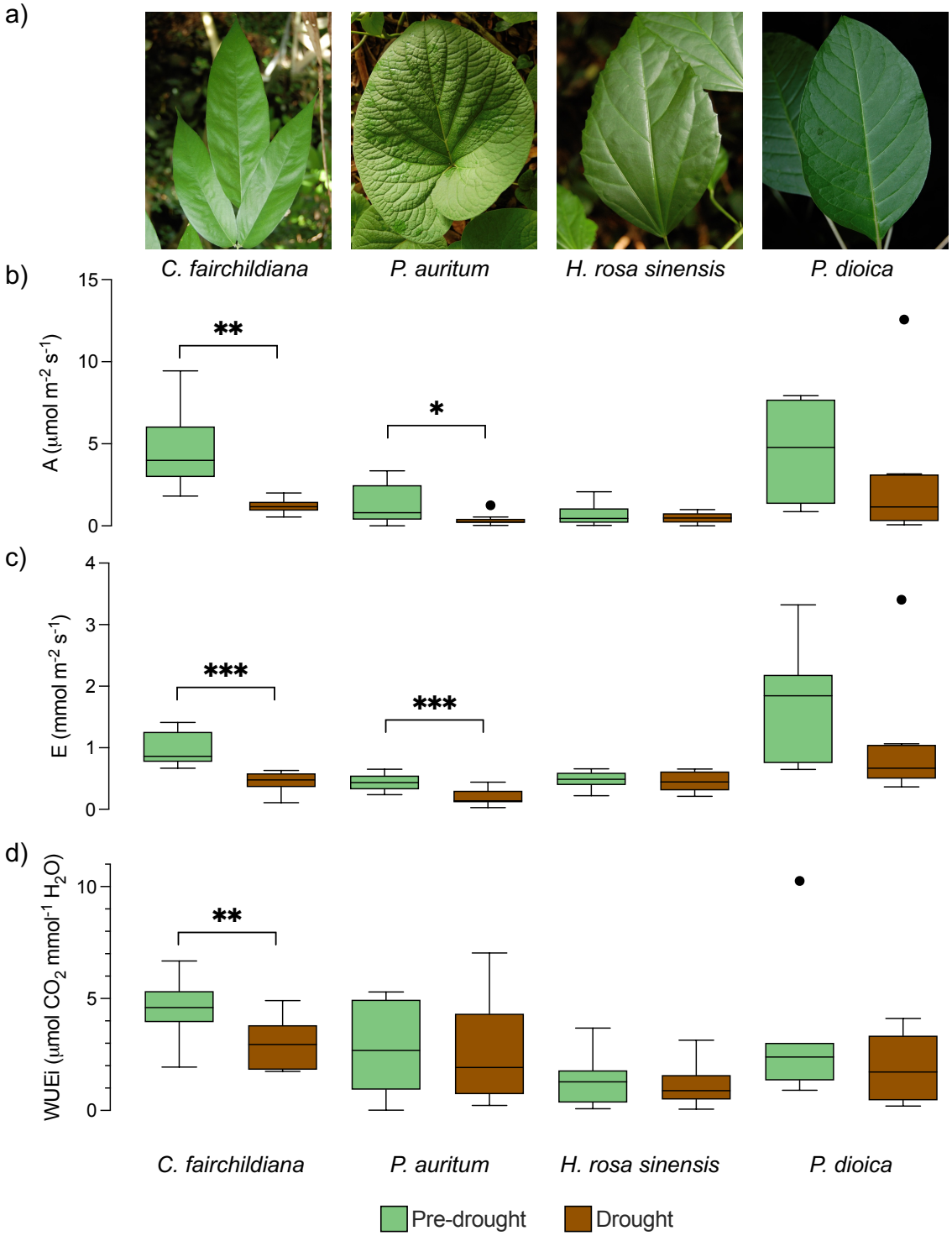

Figure 3: Representative leaves (panel a) and rates of (b) carbon assimilation A, (c) transpiration E, and (d) instantaneous water use efficiency WUEi measured on individual leaves of *Clitoria fairchildiana*, *Piper auritum, Hibiscus rosa sinensis*, and *Phytolacca dioica* under pre-drought (green) and drought (brown) conditions. Boxes represent the median and 25 – 75 % range of 7-12 replicate leaves. Whiskers and outliers calculated using Tukey's method. Significant differences between pre-drought and drought conditions for each species are indicated as * when $p < 0.05$, ** when $p < 0.01$, and *** when $p < 0.001$.

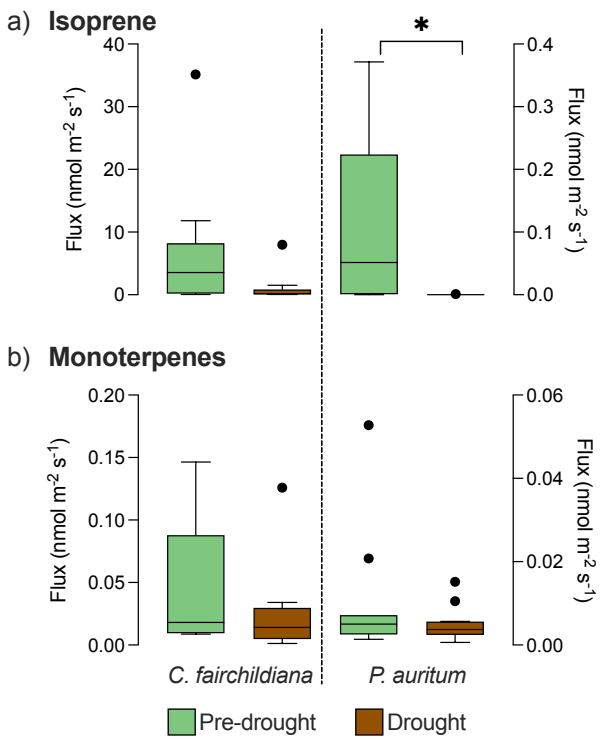

Figure 4: Emission rates of (a) isoprene and (b) monoterpenes measured on individual leaves of *Clitoria fairchildiana* and *Piper auritum* under pre-drought (green) and drought (brown) conditions. Fluxes from *C. fairchildiana* are plotted on the left y-axis and fluxes from *P. auritum* on the right y-axis. Boxes represent the median and 25 – 75 % range of 7-12 replicate leaves. Whiskers and outliers are calculated using Tukey's method. Significant differences between pre-drought and drought conditions for each species are indicated as: * when $p < 0.05$.

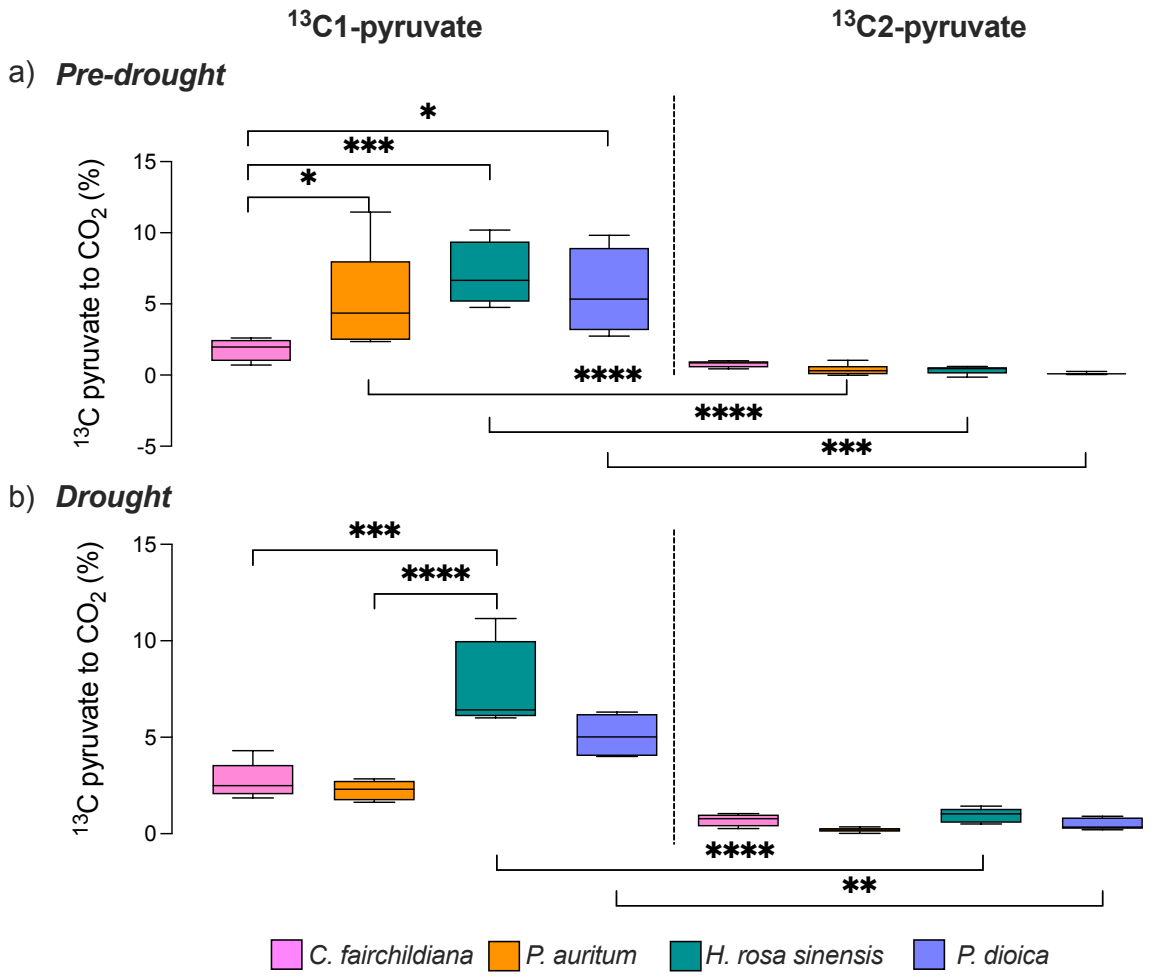

Figure 5 Percent of ^{13}C from $^{13}C1$-labeled pyruvate (left column) and $^{13}C2$-labeled pyruvate (right column) that was released as CO_2 by *Clitoria fairchildiana*, *Piper auritum, Hibiscus rosa sinensis*, and *Phytolacca dioica* under pre-drought (panel a) and drought (panel b) conditions. Boxes represent the median and 25 – 75 % range of 3 - 6 replicate leaves. Whiskers and outliers are calculated using Tukey's method. Significant differences among groups as determined by three-way ANOVA with Tukey's posthoc test are indicated as: * when $p < 0.05$, ** when $p < 0.01$, *** when $p < 0.001$, and **** when $p < 0.0001$.

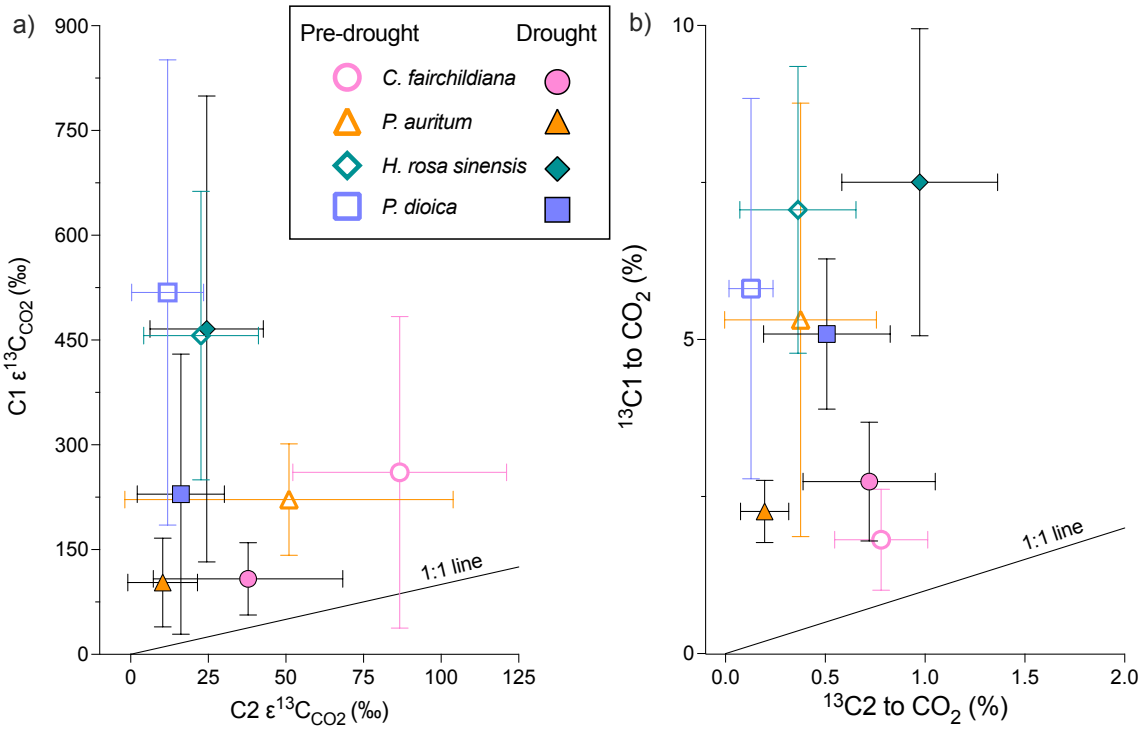

Figure 6 (a) ^{13}C enrichment of CO_2 from $^{13}C1$-labeled pyruvate (y-axis) plotted relative to ^{13}C enrichment of CO_2 from $^{13}C2$-labeled pyruvate (x-axis) during pre-drought (open symbols) and drought (closed symbols). (b) Same as panel a, but with the % of ^{13}C from each position of the pyruvate label. Symbols represent mean values and error bars represent one standard deviation of 3 – 6 replicate leaves per species.

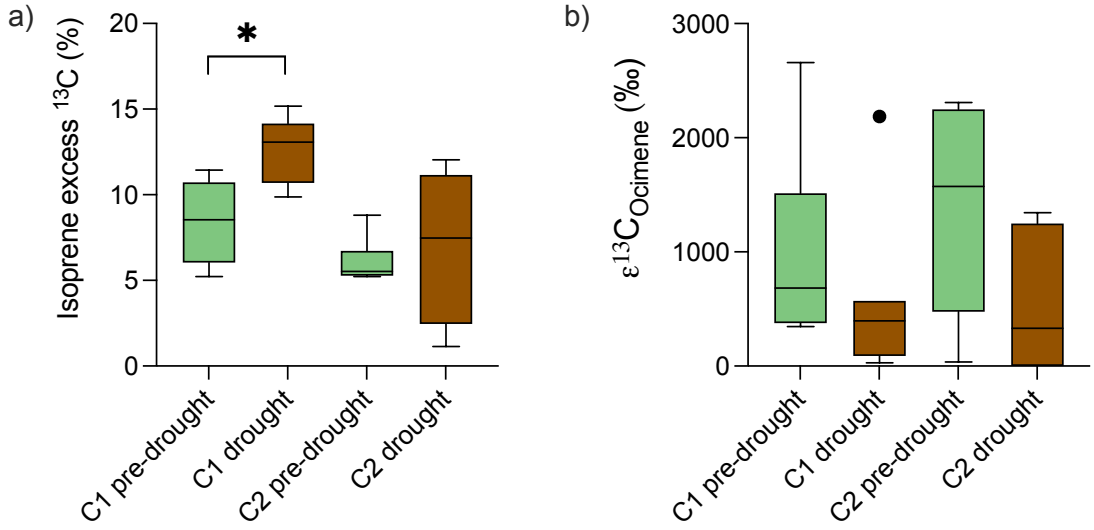

Figure 7: ^{13}C from ^{13}C-labeled pyruvate incorporation into VOCs from *Clitoria fairchildiana*. (a) ^{13}C excess isoprene emissions relative to natural background ^{13}C abundance for isoprene and (b) ^{13}C enrichment of the monoterpene trans-β-ocimene relative to unlabeled measurements during pre-drought (green) and drought (brown) (4 – 6 replicates per treatment). Boxes represent median and 25-75% range of 7-12 replicate leaves. Whiskers and outliers are calculated using Tukey's method.

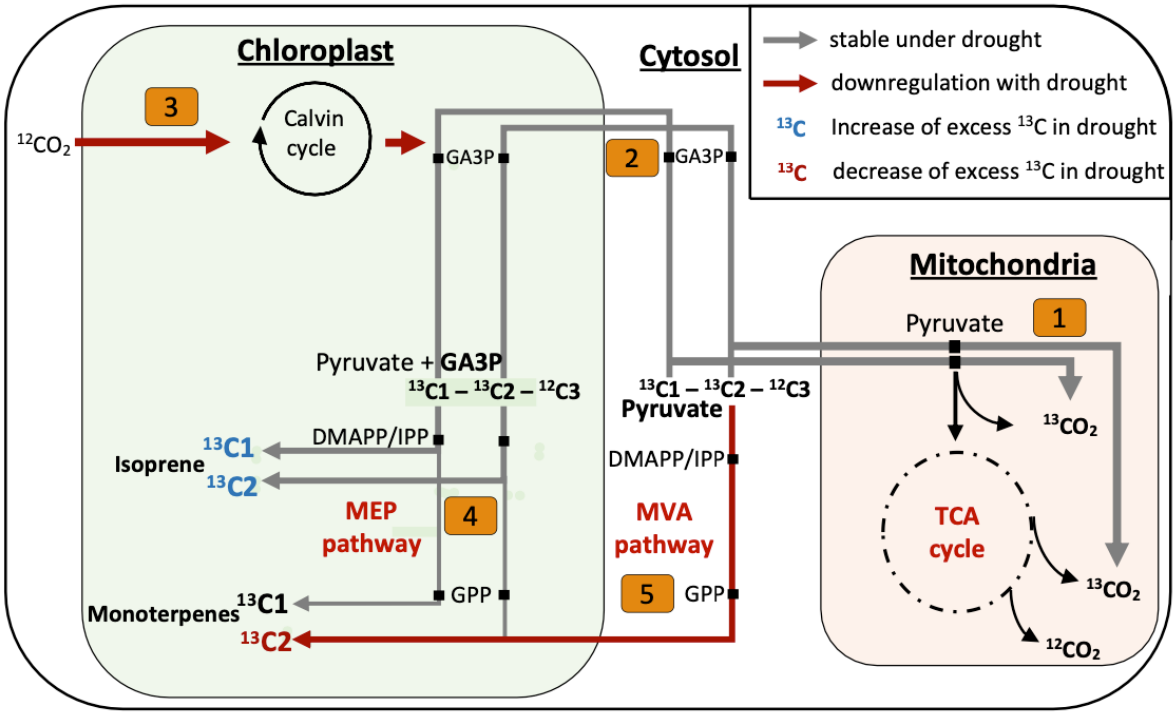

Figure 8: Schematic representation of pyruvate carbon partitioning among biosynthetic processes involved in the synthesis of isoprenoids and production of CO_2 within *Clitoria fairchildiana* cells as well as proposed adjustments of these processes during drought. Several intermediate steps and involved enzymes are removed for clarity. Arrow thickness represents the relative amount of ^{13}C1-/ ^{13}C2-labeled pyruvate used for the indicated pathway during pre-drought conditions. Gray arrows indicate no changes in carbon utilization during drought while brown arrows indicate a down-regulation of the pathway. Blue colored ^{13}C1/^{13}C2 indicate an increase in excess ^{13}C emissions of isoprene or monoterpenes during drought, while red color indicates a decline in excess ^{13}C emissions. Numbers represent the relevant pathways discussed, with descriptions of pathways 1-5 described in the caption of Figure 1. TCA, tricarboxillic acid; GA-3-P, glyceraldehyde 3-phosphate; DMAPP Dimethylallyl pyrophosphate; IPP, isopentenyl pyrophosphate; MEP, methylerythritol phosphate; GPP, geranyl pyrophosphate; MVA, mevalonic acid.

Table 1: Fluxes of the main monoterpenes emitted by *Clitoria fairchildiana*, as determined by GC-MS analysis. Monoterpene fluxes from the other three species were too low for quantification by GC-MS. Fluxes are reported as mean and standard error. [1]These two compounds co-eluted on the GC and the combined flux is reported.

	Pre-drought flux ($pmol\ m^{-2}\ s^{-1}$)		Drought flux ($pmol\ m^{-2}\ s^{-1}$)	
α-pinene	6.51	± 2.41	3.09	± 0.20
d-3-carene/ β-pinene[1]	9.28	± 2.96	5.52	± 0.46
limonene	5.10	± 0.79	4.39	± 0.23
trans-β-ocimene	5.47	± 1.20	28.88	± 7.35

Supplementary Data

Table S1: Leaf temperature inside enclosed leaf cuvettes during the experiments in comparison to ambient daytime temperature ranges inside the Biosphere 2 tropical rainforest. [1] Data from Werner *et al.*, 2021.

Species	Phase	$T_{cuvette}$ (°C)		$T_{ambient}$ (°C)[1]	
		Mean	Std	Lower limit	Upper limit
C. fairchildiana	pre-drought	30.53	± 6.81	23.3	35.0
	drought	28.83	± 2.30	22.6	34.8
P. auritum	pre-drought	24.77	± 1.53	21.3	26.6
	drought	28.25	± 1.43	22.2	29.6
H. rosa sinensis	pre-drought	27.43	± 1.87	21.3	26.6
	drought	29.89	± 1.44	22.2	29.6
P. dioica	pre-drought	28.43	± 4.60	23.3	35.0
	drought	29.61	± 2.26	22.6	34.8